PHYSICAL REVIEW B **78**, 075429 (2008)

Resonant two-color high-resolution spectroscopy of a negatively charged exciton in a self-assembled quantum dot

M. Kroner,[1] K. M. Weiss,[1] B. Biedermann,[1] S. Seidl,[1] A. W. Holleitner,[1] A. Badolato,[2] P. M. Petroff,[2] P. Öhberg,[3] R. J. Warburton,[3] and K. Karrai[1]

[1]*Center for NanoScience and Fakultät für Physik, Ludwig Maximilians Universität, 80539 München, Germany*

[2]*Materials Department, University of California, Santa Barbara, California 93106, USA*

[3]*School of Engineering and Physical Sciences, Heriot-Watt University, Edinburgh EH14 4AS, United Kingdom*

(Received 7 May 2008; published 21 August 2008)

We report high-resolution resonant two-color laser spectroscopy on single self-assembled InGaAs quantum dots. The negatively charged exciton in a quantum dot can decay radiatively into both electron-spin ground states, the states with an electron in the quantum dot with its spin parallel or antiparallel to an applied magnetic field. The two decay paths can be used for optical spin alignment via optical pumping. We apply two laser fields at two different colors resonant with the two Zeeman split optical transitions to study the properties of the spin of the resident electron in the quantum dot in both the Faraday and Voigt geometries. The resonant two-color signal is monitored as a function of the laser power as well as the applied magnetic and electric field allowing us to determine spin decay and dephasing rates. We find the rate at which the optical spin alignment can be performed depending on the direction and the magnitude of the applied magnetic field. Finally we demonstrate the feasibility of performing coherent all-optical spin manipulation of an electron spin in a quantum dot.

DOI: 10.1103/PhysRevB.78.075429 PACS number(s): 73.21.La, 78.67.Hc, 71.35.Ji

I. INTRODUCTION

The spin of an electron or a hole confined to a low-dimensional solid-state quantum system is a promising candidate for realizing a qubit, the fundamental building block of quantum based information processing devices.[1,2] This is mainly due to the long spin coherence and lifetimes that have been observed in self-assembled quantum dots (QD).[3,4] The initial step qubit initialization can be achieved by optical spin pumping (OSP). Furthermore, probing optical pumping as a function of the system parameters, applied electric and magnetic fields, pumping power, etc. is a powerful way of studying the spin relaxation and decoherence mechanisms at the single dot level.[5–8] For instance, in QDs at low magnetic fields, optical pumping experiments have shown that electron-spin relaxation is dominated by the hyperfine interaction, whereas at high magnetic fields electron-spin relaxation is limited by spin-orbit coupling.[8] It is worth noting that little is known so far about the nuclear-spin dynamics in QDs.[9,10] The inhomogeneous strain in a self-assembled quantum dot strongly influences the Overhauser field fluctuations and hence the electron-spin dynamics.[11] In optically detected single electron-spin-resonance experiments, which utilize OSP for spin initialization, there are clear manifestations of Overhauser field fluctuations.[12]

In this paper we present insights into optical pumping, spin relaxation, and spin decoherence from optical experiments on single quantum dots in both the Faraday and Voigt geometries. The crucial tool is the use of two optical lasers pumping two different transitions. The results are analyzed in the framework of a quantum optical model allowing us to deduce the electron-spin relaxation and dephasing rates. Furthermore, we describe a method to manipulate optically the electron spin in a coherent way: we present a scheme that will eventually allow the application of coherent spin manipulation, known from atom optics, based on the optically induced coherence between two ground states coupled to a common excited state.

II. METHODS

A. Sample

We study single InGaAs QDs embedded in a field effect device.[13] This allows us to charge the quantum dot in a controlled way with single electrons[14–16] simply by applying a gate voltage to the sample. As a back gate we have a two-dimensional electron gas (2DEG) (charge-carrier density $n_e = 1.2\times10^{12}$ cm^2 and mobility $\mu_e = 8.1\times10^3$ cm^2/V s), separated from the QD layer by a 25-nm-thick tunnel barrier of intrinsic GaAs. The QD layer is buried 251 nm below the surface of the sample, on which a semitransparent metallic (5-nm NiCr) top gate is deposited, yielding a lever arm $\eta = 12$.[14,16] The electrostatic energy of the electronic QD state is then $E_{\mathrm{el}} = e(V_g + V_g^0)/\eta$, with the applied gate voltage V_g and the inbuilt Schottky voltage $V_g^0 = 0.62$ V. An AlAs-GaAs superlattice between the QD layer and the sample surface prohibits leakage currents to the top gate. Choosing the applied bias V_g such that the electronic conduction state of the QD is shifted just below the Fermi energy of the 2DEG, an electron is trapped in the QD via tunneling from the back contact. For a second electron to tunnel into the QD, the Coulomb repulsion energy has to be overcome and hence there is a voltage range extending over ≈ 0.25 V, in which the QD ground state is charged with a single electron.[13–16]

B. Resonant laser spectroscopy

The sample is mounted in a fiber based confocal microscope, which itself is located in a hermetically sealed thin

walled stainless steel tube filled with a small amount of He exchange gas (~30 mbar at room temperature). To operate at 4.2 k, the whole setup is immersed in a liquid He bath cryostat, which is equipped with a superconducting coil to generate magnetic fields up to 9 T.[17–20] The sample is positioned in the focus of the microscope objective ($NA=0.55$) using low-temperature positioners for all three axes. In this way, a single QD can be chosen from the ensemble *in situ* and kept reliably in the focus of the microscope for the duration of the experiment. Due to the diffraction-limited focal spot (~1.2 μm) and the low QD density on the sample, it is possible to have only one single QD in the illuminated area. For illumination, a tunable narrow-band laser is used (linewidth <3 MHz and $\lambda=930-990$ nm) and the transmitted light is detected by a Si photodetector mounted directly behind the sample at 4.2 K. When the laser light is resonant with the excitonic transition, the QD acts as a scatterer, and we detect the resonant Rayleigh scattering in the forward direction as a change in the transmitted light.[21–23] For noise reduction, a modulation technique with lock-in detection is used. We exploit the quantum confined Stark effect to control the QD resonance energy via an applied bias.[22] The gate voltage is modulated with a square wave ($V_{pp}=100$ mV and $f=77$ Hz), while a dc voltage offset is swept to measure the differential transmission as a function of the detuning of the exciton resonance relative to the laser photon energy, which is kept constant. Alternatively, the gate voltage is kept constant, apart from the modulation, and the laser photon energy is swept. In Fig. 1(a) a transmission spectrum is shown for a single negatively charged QD. The corresponding optical transition is illustrated in Fig. 1(b) with and without magnetic field. The laser drives the transition, and at high enough laser fluence it leads to a power broadening of the resonance line. The spontaneous relaxation rate Γ corresponds to the lifetime-limited linewidth.[23–25]

The measured signal is the transmission through the sample ($\Delta T/T$) as it is shown in Figs. 1(a) and 1(c). In the following we will also refer to the transmission contrast $\alpha=1-\Delta T/T$ as it is defined in Refs. 22 and 21

On applying a magnetic field, the unpolarized resonance line of the negatively charged exciton splits into two resonances.[26,27] The two resonances can be excited by left-handed and right-handed circularly polarized light,[20] as shown on the right of Fig. 1(b). The splitting is given by $\Delta_X=g_X\mu_B B$, with the excitonic g factor $g_X=g_e+g_h$, the sum of the electron and hole g factors in the QD. In Fig. 1(c) a spectrum of a negatively charged exciton in a magnetic field is shown for linearly polarized excitation. The Zeeman split resonances are separated by $\Delta_X=51.7$ μeV corresponding to an excitonic g factor $g_X=-1.80\pm0.01$.

III. SPIN DEPENDENT LASER SPECTROSCOPY

A. Optical spin pumping

Optical spin pumping of a resident electron in a QD was pioneered by Atatüre *et al.*[5] and studied in detail by Dreiser *et al.*[8] OSP was successfully used as the basis for single electron-spin-resonance experiments.[12] A description is given here to introduce the optical transitions and their rates. Here

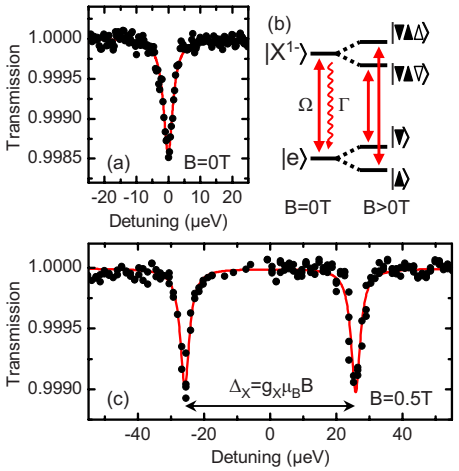

FIG. 1. (Color online) High-resolution resonant laser spectroscopy on a single QD in Faraday geometry. The data were recorded on dot A. In (a) the unpolarized resonance line of a QD charged with one electron is shown against energy detuning. The change in transmission through the sample of a narrow-band laser is measured, while the exciton resonance is detuned from the laser photon energy by the dc Stark shift. The transition is depicted in (b) on the right side with no applied magnetic field. The resonant laser drives the transition with a Rabi frequency Ω, while the exciton decays spontaneously with rate Γ. On the right side of (b) the transitions of a negatively charged exciton are shown, with a magnetic field applied along the growth direction. The ground and excited states are split by the Zeeman energy. A transmission spectrum for a magnetic field of 0.5 T is shown in (c). The laser was linearly polarized to resolve both Zeeman split resonances. The energy difference between the two resonances corresponds to the sum of the Zeeman splittings of the excited and ground states. As depicted in (b) the Zeeman splitting of the exciton is determined by the hole and the Zeeman splitting of the ground state is determined by the electron. The lines are Lorentzian fits to the data, yielding a linewidth at half maximum of ≈3.5 μeV.

the tunneling interaction between the QD and the back contact was reduced relative to the original sample design in Refs. 13 and 14 by reducing the density of states in the two-dimensional (2D) back contact, in contrast to the earlier work[5,8] where the tunneling barrier thickness from the QD to the n-doped three-dimensional (3D) back contact was increased.

In an external magnetic field, the Zeeman split ground and excited states of the X^{1-} exciton, as depicted in Fig. 1(b), represent a four-level system. In the Faraday geometry the magnetic field is applied along the sample growth axis. Optical selection rules allow the two circularly polarized transitions $|\blacktriangle\rangle\leftrightarrow|\blacktriangle\blacktriangledown,\triangle\rangle$ for σ^+ polarization and $|\blacktriangledown\rangle\leftrightarrow|\blacktriangle\blacktriangledown,\triangledown\rangle$ for σ^- polarization. A relaxation of the selection rules also allows weakly the decay into the ground states with opposite electron spin, $|\blacktriangle\blacktriangledown,\triangle\rangle\rightsquigarrow|\blacktriangledown\rangle$ and $|\blacktriangle\blacktriangledown,\triangledown\rangle\rightsquigarrow|\blacktriangle\rangle$, the "forbidden" transitions. The hole spin lifetime has been reported to be of the order of 1 ms at low magnetic fields.[7,28] Hence, the forbidden transition is mediated by the hyperfine interaction with the nuclei in the QD and by heavy-hole light-hole mixing and not by a hole spin-flip process followed by excitonic recombination (e.g., $|\blacktriangle\blacktriangledown,\triangle\rangle\rightarrow|\blacktriangle\blacktriangledown,\triangledown\rangle|\blacktriangledown\rangle$).[5]

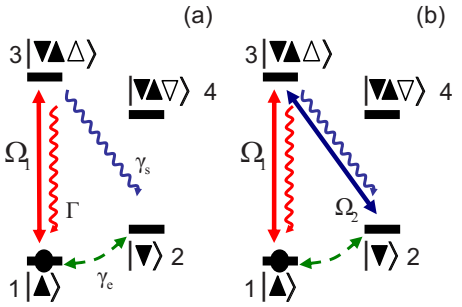

FIG. 2. (Color online) Level schemes of a negatively charged QD in a magnetic field. In (a) the transitions responsible for the OSP are shown. A laser pumps resonantly the transition $|1\rangle \leftrightarrow |3\rangle$ with Rabi frequency Ω_1 and creates an exciton. The exciton decays spontaneously into the ground state $|1\rangle$ and $|2\rangle$ at rate Γ and γ_s, respectively, where transition rate $\gamma_s \ll \Gamma$ such that we label transition $|2\rangle \leftrightarrow |3\rangle$ as a forbidden transition. The spin-flip rate γ_e leads to a relaxation of the spin polarization toward equal population of the two states $|1\rangle$ and $|2\rangle$. In (b) the two laser, repump scheme is shown. An additional laser pumps resonantly the forbidden transition $|2\rangle \leftrightarrow |3\rangle$, with Rabi frequency Ω_2. This leads to a transfer of ground-state population from $|2\rangle$ to $|1\rangle$ and hence frustrates the OSP.

By pumping one of the optically allowed transitions resonantly, e.g., $|\blacktriangle\rangle \leftrightarrow |\blacktriangle\blacktriangledown, \triangle\rangle$, with a Rabi frequency Ω_1 as depicted in Fig. 2(a), the electron spin eventually becomes trapped in the $|\blacktriangledown\rangle$ state by undergoing a forbidden transition at a rate γ_s.[5] The optical spin pumping fidelity $\vartheta = (n_2 - n_1)/(n_2 + n_1)$, where $n_{1,2}$ is the population of the state $|\blacktriangle\rangle$ and $|\blacktriangledown\rangle$, respectively, is limited by the ratio of the forbidden transition rate γ_s at which the state $|\blacktriangledown\rangle$ is populated and the spin-flip rate γ_e. Equilibrium corresponds to $n_1 = n_2 = 0.5$ in the case here where $g_e \mu_B B \ll k_B T$.[20] We measure the change in transmission due to absorption of the laser that is resonantly driving the transition $|\blacktriangle\rangle \leftrightarrow |\blacktriangle\blacktriangledown, \triangle\rangle$. In case of spin pumping, the Boltzmann distributed population of the ground states is strongly modified and the probability for the electron to be in the $|\blacktriangle\rangle$ state is reduced; $n_1 < 0.5$. Since the transmission signal is a measure of the population of the ground state,[20] the signal is also reduced.[5,6] We get a simple expression for the spin pumping fidelity from rate equations;

$$\vartheta \approx \frac{1}{1 + 4\frac{\gamma_e}{\gamma_s}}, \tag{1}$$

which we use to estimate the transmission signal α as

$$\alpha \approx \alpha_0 (1 - \vartheta), \tag{2}$$

where α_0 is the transmission signal for equal population of the two ground states, e.g., in case of $B = 0$.

In Fig. 3(a) the normalized transmission contrast is plotted for the X^{1-} over the whole gate voltage range where the single electron state is stable.[16] At $B = 0$ where OSP is suppressed between the two charging voltages, the transmission contrast is constant. At voltages below −0.975 V, where the ground state is the empty QD, and at voltages above −0.75 V, where a second electron tunnels into the dot, the transmission contrast drops to zero. The amplitude of the

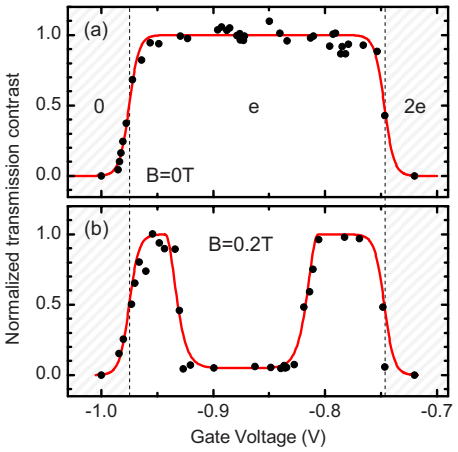

FIG. 3. (Color online) Measured transmission contrast versus gate voltage, over the charging plateau, where the QD contains one resident electron, e. The data were recorded on Dot A. The transmission is normalized to the maximum contrast on the plateau. (a) The X^{1-} plateau with no magnetic field applied. At the edges toward the empty (zero) and doubly negatively charged QD (2e), the transmission contrast decays following Eq. (4) (line), corresponding to a temperature $T = 4.2$ K. In (b) the transmission contrast is plotted in the same gate voltage range, with a magnetic field of 0.2 T applied. In the middle of the plateau the OSP leads to a drastic reduction in the transmission contrast. The line is a fit to the data of a product of Eq. (2) using Eq. (1) to describe ϑ and Eq. (5) to calculate the gate voltage dependent spin-flip rate γ_e ($\hbar\Gamma_{\text{tun}} = 0.05$ μeV).

transmission signal over the plateau edge maps the probability of finding one electron (the ground state of the probed optical transition) in the QD. At the low bias edge, the probability of finding a single electron in the QD is

$$f(E) = \frac{1}{1 + e^{E - E_F/k_B T}}, \tag{3}$$

where $T = 4.2$ K is the temperature and E_F is the Fermi energy. At the low bias edge, the transmission contrast is then

$$\alpha = \alpha_0 f[E_{\text{el}}(V)]. \tag{4}$$

Here $E_{\text{el}}(V) = e(V_1 - V)/\eta$ is the electrostatic energy of the electron in the QD setting $E_F = 0$ with lever arm $\eta = 12$.[14,16] V_1 is the voltage at which the empty and singly charged QD states are degenerate. Similar results pertain to the high bias edge of the plateau close to the transition between the singly and doubly occupied quantum dot states. The overall result for α, symmetric about the plateau center, is plotted in Fig. 3(a). The only fit parameters are the charging voltages for the first electron V_1 and the second electron V_2. The quality of the fit proves that the QD temperature is indeed the bath temperature in this experiment.

Repeating this experiment with an external magnetic field of $B = 0.2$ T yields the result shown in Fig. 3(b). While at the edges of the plateau, the amplitude of the transmission contrast is similar to the zero-field situation; in the middle of the plateau, the signal is strongly suppressed, a signature of OSP. In the middle of the plateau, the spin of the resident electron is optically pumped into the $|\blacktriangledown\rangle$ state.[5,6] At the edges of the

plateau, the electronic state of the first electron in the QD for the left edge and the state for the second electron in the QD for the right edge, are energetically close to the Fermi energy. This allows cotunneling events consisting of a spin swap between the QD electron and an electron in the back contact such that the spin information of the QD electron is rapidly lost.[5,8,29] To describe the gate voltage dependency of this effect, we use the expression for the cotunneling rate γ_{cot} from the work of Smith *et al.*;[29]

$$\gamma_{\mathrm{cot}} = \frac{\hbar\Gamma_{\mathrm{tun}}^2}{2\pi}\int_{\epsilon}\left|\frac{1}{E_{\mathrm{el}}(V_1)+\epsilon+\frac{i}{2}\hbar\Gamma_{\mathrm{tun}}} + \frac{1}{-E_{\mathrm{el}}(V_2)-\epsilon+\frac{i}{2}\hbar\Gamma_{\mathrm{tun}}}\right|^2 f(\epsilon)[1-f(\epsilon)]\mathrm{d}\epsilon. \quad (5)$$

The solid line in the plot in Fig. 3(b) is a guide to the eye, based on an evaluation of Eq. (5) with the tunneling energy $\hbar\Gamma_{\mathrm{tun}}=0.05$ μeV, which is very similar to the values obtained for similar structures.[8,29] We assume it to be constant over the charging plateau. In general, for small magnetic fields, where the spin phonon interaction is weak,[4,8] the spin relaxation rate is composed of the sum of the cotunneling rate γ_e and the gate voltage independent hyperfine spin-flip rate γ_{hf};

$$\gamma_e = \gamma_{\mathrm{cot}} + \gamma_{\mathrm{hf}}. \quad (6)$$

Using this equation with a constant $\gamma_{\mathrm{hf}}=0.1$ MHz, expression (2) and the gate voltage dependency of γ_{cot} as discussed above, we obtain the behavior of the transmission signal in the middle of the plateau as a function of the gate voltage, as shown by the line in Fig. 3(b). Here $\gamma_s=50$ MHz was obtained by fitting the curve to the data points. This transition rate for the weak transition should be compared with $\Gamma=1.2$ GHz, which we obtain by power broadening analysis.[25]

Strictly, only the ratio between the spin-flip rate and the forbidden transition rate can be gained by fitting Eq. (2) to the data. To gain a more precise knowledge of the magnitude of the spontaneous decay rate of the forbidden transition γ_s, as well as all the other transition rates involved in the system, we turn now to a two-laser spectroscopy scheme.

B. Optical pumping of the forbidden transition

The weakly allowed forbidden transition depicted in Fig. 2(a) obviously leads to a decay of the excited state $|\blacktriangle\blacktriangledown,\triangle\rangle$ to state $|\blacktriangledown\rangle$, on emission of a photon. The decay rate is very small and its emission was not directly detectable in a photoluminescence experiment. However, using the transmission signal of the pump laser, a sensitive tool exists to measure the population of the state $|\blacktriangledown\rangle$. To measure the forbidden decay rate, we use a second laser, resonant with the forbidden transition, to "repump" the electron from the shelving state $|\blacktriangledown\rangle$ to the excited state $|\blacktriangle\blacktriangledown,\triangle\rangle$ of the pumping laser cycle. The pumping scheme is shown in Fig. 2(b). Monitoring the transmission signal of the pump laser, we expect an increase in the signal when the repump laser is resonant with the forbidden transition.[12] In Fig. 4 two gate voltage scans are shown. The open circles represent the transmission signal

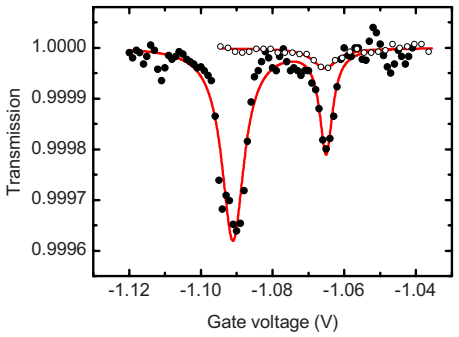

FIG. 4. (Color online) Transmission spectra in the OSP regime of the X^{1-} gate voltage range, close to the cotunneling regime. The data were recorded on Dot B. The open circles are obtained from a one-laser transmission experiment at a magnetic field of 0.5 T with circular polarization. The weak remaining signal at $V_G=-1.065$ V arises because cotunneling suppresses OSP sufficiently. At the center of the charging plateau the signal is too weak to be resolved in the noise. According to the pump scheme in Fig. 2, a second linearly polarized laser is focused on the sample. The photon energy of this second laser is chosen such that at a gate voltage of $V_G=-1.065$ V, the laser photons are resonant with the forbidden transition. The experiment is repeated: the transmission is monitored as the gate voltage is scanned while the photon energy of the two lasers remains constant. At the gate voltage where in the one-laser experiment a faint resonance is observed, an enhanced signal appears in the two-laser experiment. At an $\approx$25 mV more negative gate voltage, a second resonance becomes visible, originating from the second laser, whose energy in this case matches the excitonic transition $|\blacktriangle\rangle\leftrightarrow|\blacktriangle\blacktriangledown,\triangle\rangle$ at this gate voltage. The resonance condition of the second laser with the excitonic transition falls into the cotunneling regime, yielding a strong resonance. The gate voltage differs from that in Fig. 3 because the experiment was performed on a different QD. To check the symmetry of the pumping scheme, the experiment was repeated on the low-energy Zeeman branch, yielding the same behavior (data not shown).

measured for the pump laser only driving at gate voltage $V_g=-1.065$ V the transition $|\blacktriangle\rangle\leftrightarrow|\blacktriangle\blacktriangledown,\triangle\rangle$ with a Rabi frequency Ω_1, Fig. 2(a). The experiment was performed at an external field of $B=0.5$ T, a magnetic field at which, for an optical resonance in the middle of the plateau, the transmission signal is so strongly reduced due to OSP that it cannot be resolved in the noise. For the spectrum in Fig. 4, the laser photon energy was chosen such that the resonance occurs close to the cotunneling regime, such that it can still be resolved above the noise level. The solid dots in Fig. 4 represent the signal measured with a second laser. The second laser is resonant with the forbidden transition $|\blacktriangledown\rangle\leftrightarrow|\blacktriangle\blacktriangledown,\triangle\rangle$ with a Rabi frequency Ω_2. The resonance condition is fulfilled at a gate voltage $V_g=-1.065$ V. An increase by a factor 5 in the transmission signal of the pump laser resonantly driving the $|\blacktriangle\rangle\leftrightarrow|\blacktriangle\blacktriangledown,\triangle\rangle$ transition is observed. The enhanced signal arises due to the repump of the electron into the pumping cycle of the first laser as shown in Fig. 2(b). Experiments with only the second laser reveal that the scattering of photons by resonantly pumping the forbidden transition cannot be resolved (data not shown here).[12] At more negative gate voltages ($V_g=-1.09$ V) a second resonance peak is observed in the spectrum measured with two

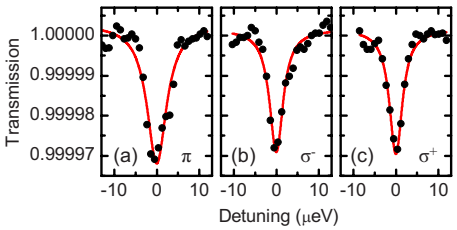

FIG. 5. (Color online) Two color, repump spectra of the $|\blacktriangle\rangle \leftrightarrow |\blacktriangle\blacktriangledown, \triangle\rangle$ transition by pumping the $|\blacktriangledown\rangle \leftrightarrow |\blacktriangle\blacktriangledown, \triangle\rangle$ forbidden transition with differently polarized laser fields. The data were recorded on Dot B. In (a) the second laser was linearly polarized, according to the linear polarization basis defined by the neutral exciton fine structure splitting. In (b) and (c) the second laser field is left-handed and right-handed circularly polarized, respectively. The circular polarization basis was defined by one color spectroscopy on the X^{1-} in a magnetic field (Ref. 21). No effect of the repumping signal on the polarization of the repump laser is observed. The laser pumping the $|\blacktriangle\rangle \leftrightarrow |\blacktriangle\blacktriangledown, \triangle\rangle$ transition was σ^+ polarized. The lines are Lorentzian fits to the data.

lasers. This resonance is also observed for a gate voltage scan with only the second laser and it originates from a resonance of the laser with the $|\blacktriangle\rangle \leftrightarrow |\blacktriangle\blacktriangledown, \triangle\rangle$ transition, which is fulfilled for the given laser photon energy at this particular gate voltage. Since the resonance condition lies at a lower gate voltage, it takes place in the cotunneling regime where spin pumping does not reduce the transmission amplitude. From the gate voltage difference between the two peaks, the linear Stark effect, as well as the photon energy differences of the two laser fields, the Zeeman splitting of the electronic ground state can be calculated to be $E_{Z,e}=g_e\mu_B B = 23.1$ μeV, which corresponds to an electronic g factor $g_e = -0.70 \pm 0.01$.[12] The sign of the g factor has been obtained from earlier polarization sensitive absorption measurements on an X^{1-} in a magnetic field.[20]

C. Polarization dependence

We comment on the polarization properties of the two laser signal. The transmission contrast of the pump laser, which is circularly polarized σ^+ to match the optical selection rule for the transition $|\blacktriangle\rangle \leftrightarrow |\blacktriangle\blacktriangledown, \triangle\rangle$, is measured for different polarizations of the repump laser, resonant with the $|\blacktriangledown\rangle \leftrightarrow |\blacktriangle\blacktriangledown, \triangle\rangle$ forbidden transition. Figure 5 shows that the repump signal is equally strong for linear (π) and both circular (σ^+ and σ^-) polarizations. The finding suggests that, at least at 0.5 T, the field used in the experiment, the forbidden transition is unpolarized. This is somewhat surprising: candidate mechanisms for allowing the forbidden transition are electron-spin mixing induced by the hyperfine interaction or possibly heavy-hole light-hole mixing both of which, at the simplest level of approximation, should result in a σ^+-polarized forbidden $|\blacktriangledown\rangle \leftrightarrow |\blacktriangle\blacktriangledown, \triangle\rangle$ transition. Generally speaking, a more detailed study of the polarization properties of the repump signal at different magnetic fields is necessary to gain deeper insight into the mechanisms leading to the breaking of the selection rules and hence to the finite oscillator strength of the forbidden transition.

In the following experiments the laser pumping the $|1\rangle \leftrightarrow |3\rangle$ transition is σ^+ polarized, while the other laser is linearly polarized, to gain a consistent set of data.

IV. QUANTUM OPTICS OF THE X^{1-} STATE AT A FINITE MAGNETIC FIELD

The ability to perform resonant two-laser absorption experiments on the λ system, formed by the X^{1-} in a magnetic field, allows us to obtain a comprehensive understanding of the involved rates and their physical origin. To do this, we first develop a quantum optical description of the three-level system in Fig. 2(b). Then we show results of the spin repump experiment as a function of gate voltage, magnetic field, and laser power to gain access to the rates connecting the electronic and excitonic states of the X^{1-}.

A. Quantum optical model

To describe the experiments in Secs. V and VI, we derive a master equation for the density matrix for the three-level system of an X^{1-} in a magnetic field. In Sec. IV B the density matrix is linked to the resonant laser spectroscopy experiment.

The λ system of the X^{1-} in a magnetic field is formed out of two ground states, $|1\rangle \equiv |\blacktriangle\rangle$ and $|2\rangle \equiv |\blacktriangledown\rangle$, with energies, $E_1=0$ and $E_2=\hbar\omega_{12}$, and the excited state $|3\rangle \equiv |\blacktriangle\blacktriangledown, \triangle\rangle$ with energy $E_3=\hbar\omega_{13}$. The energy $E_2=|g_e|\mu_B B \approx 20$ μeV is the Zeeman splitting of the electronic state in the QD, while the energy of the excited state E_3 is around ≈ 1.2 eV. The states $|1\rangle$ and $|3\rangle$, and $|2\rangle$ and $|3\rangle$ are coupled by two coherent laser fields with angular frequencies ω_1 and ω_2, respectively, as depicted in Fig. 2(b) by the straight arrows. The Hamilton operator of the system is

$$\hat{H} = \hat{H}_0 + \hat{H}_{\text{opt}}, \tag{7}$$

with the Hamilton operator of the unperturbed system,

$$\hat{H}_0 = \hbar\omega_{12}|2\rangle\langle 2| + \hbar\omega_{13}|3\rangle\langle 3|. \tag{8}$$

We use a semiclassical ansatz in which the light fields are treated classically and the QD quantum mechanically. The light fields induce a dipole moment in the QD. We take the electromagnetic fields of the light waves as oscillating parallel to the excitonic dipole moment in the QD so that $\mathbf{F}(\mathbf{r},t) = F_i \cos(\omega_i t)\mathbf{F}(\mathbf{r}) \rightarrow F = F_i \cos(\omega_i t)$, where $i=1,2$.[30] By defining the Rabi frequencies (assumed real) as $\Omega_i = \frac{D_{i3}F_i}{\hbar}$, where $i=1,2$, we write the Hamilton operator for the light fields as

$$\hat{H}_{\text{opt}} = \frac{\hbar\Omega_1}{2}(e^{i\omega_1 t}|1\rangle\langle 3| + e^{-i\omega_1 t}|3\rangle\langle 1|) + \frac{\hbar\Omega_2}{2}(e^{i\omega_2 t}|2\rangle\langle 3| + e^{-i\omega_2 t}|3\rangle\langle 2|). \tag{9}$$

Fast oscillating terms are neglected, based on the rotating wave approximation, since the laser frequency is close to the resonance frequency of the dipole transition.[31] The Schrödinger equation $\hat{H}\psi = i\hbar\partial_t\psi$ for the wave function $|\psi\rangle$

$=\Sigma_i c_i|i\rangle$ can be written in the basis of the QD states $|i\rangle i=1,..,3$ as

$$\hat{H}=\frac{1}{2}\hbar\begin{pmatrix}0 & 0 & \Omega_1 e^{i\omega_1 t}\\ 0 & 2\omega_{12} & \Omega_2 e^{i\omega_2 t}\\ \Omega_1 e^{-i\omega_1 t} & \Omega_2 e^{-i\omega_2 t} & 2\omega_{13}\end{pmatrix}. \tag{10}$$

Both optical couplings, $|1\rangle\leftrightarrow|3\rangle$ and $|2\rangle\leftrightarrow|3\rangle$, are treated nonperturbatively. To eliminate the time dependence from the Hamiltonian, we choose a rotating frame:

$$c_1=\tilde{c}_1,$$

$$c_2=\tilde{c}_2 e^{-\mathrm{i}(\omega_1-\omega_2)t},$$

$$c_3=\tilde{c}_3 e^{-\mathrm{i}\omega_1 t}. \tag{11}$$

Introducing the detunings,

$$\delta_1=\omega_{13}-\omega_1,$$

$$\delta_2=\omega_{23}-\omega_2, \tag{12}$$

we obtain the time independent Hamilton operator in the rotating frame,[32]

$$\hat{\tilde{H}}=\frac{1}{2}\hbar\begin{bmatrix}0 & 0 & \Omega_1\\ 0 & 2(\delta_1-\delta_2) & \Omega_2\\ \Omega_1 & \Omega_2 & 2\delta_1\end{bmatrix}. \tag{13}$$

The Hamiltonian $\hat{\tilde{H}}$ describes the coherent evolution of the QD with the two-laser fields. However, decay processes are clearly important. The excited state $|3\rangle$ decays radiatively into the ground state $|1\rangle$ at rate Γ and into state $|2\rangle$ at rate γ_s. Rate γ_e describes spin-flip processes between states $|1\rangle$ and $|2\rangle$ with no preferred direction for small magnetic fields since $|g_e\mu_B B|\ll k_B T$, i.e., spin decays $|1\rangle\rightarrow|2\rangle$ and $|2\rangle\rightarrow|1\rangle$ have the same rate. Furthermore, the electron spin can dephase without relaxing, i.e., we introduce a dephasing rate γ_2, describing the pure dephasing of $|2\rangle$ with respect to $|1\rangle$. In state $|3\rangle$ pure dephasing is omitted since the spontaneous emission rate dominates the recombination process. We include the decoherence terms in the Lindblad form,[30]

$$\begin{aligned}L\rho=&\sum_{i,j}\frac{1}{2}\gamma_{ij}[2|j\rangle\langle i|\rho|i\rangle\langle j|-(|i\rangle\langle i|\rho+\rho|i\rangle\langle i|)]\\ =&\frac{1}{2}\Gamma(2|1\rangle\langle 3|\rho|3\rangle\langle 1|-|3\rangle\langle 3|\rho+\rho|3\rangle\langle 3|)\\ &+\frac{1}{2}\gamma_s(2|2\rangle\langle 3|\rho|3\rangle\langle 2|-|3\rangle\langle 3|\rho+\rho|3\rangle\langle 3|)\\ &+\frac{1}{2}\gamma_e(2|1\rangle\langle 2|\rho|2\rangle\langle 1|-|2\rangle\langle 2|\rho+\rho|2\rangle\langle 2|)\\ &+\frac{1}{2}\gamma_e(2|2\rangle\langle 1|\rho|1\rangle\langle 2|-|1\rangle\langle 1|\rho+\rho|1\rangle\langle 1|)\\ &+\frac{1}{2}\gamma_2(2|2\rangle\langle 2|\rho|2\rangle\langle 2|-|2\rangle\langle 2|\rho+\rho|2\rangle\langle 2|).\end{aligned} \tag{14}$$

With this the master equation for the density matrix $\rho_{ij}=\tilde{c}_i\tilde{c}_j$ is given by

$$i\frac{d\rho_{ij}}{dt}=\frac{1}{\hbar}\sum_{k=1}^{3}(\tilde{H}_{ik}\rho_{kj}-\rho_{ik}\tilde{H}_{ik})+i(L\rho)_{ij}. \tag{15}$$

B. Connection to the experiment

In the experiment we measure the differential transmission of the laser field resonant with the transition $|1\rangle\leftrightarrow|3\rangle$. At resonance, the laser induces resonant Rayleigh scattering from the QD. At the detector, there are two fields: the laser field and the Rayleigh field. The experimental signal on the detector arises from a time-averaged interference of these two fields.[23] The differential transmission signal is given by[23]

$$\frac{\Delta T}{T}=1-\left\langle\frac{|F_1+F_s|^2}{|F_1|^2}\right\rangle. \tag{16}$$

Here F_1 is the electric field of the pump laser and F_s is the Rayleigh scattered field from the QD. Since the experiment measures the steady state of the interference, the square modulus of the electric-field components is time averaged, indicated by the brackets. F_s is proportional to the derivative of the oscillating dipole moment D_{13}, which is itself connected to the density-matrix element ρ_{13},[31]

$$F_s=\frac{eD_{13}}{2A\epsilon_0 cn}i\omega_1(\rho_{31}e^{-i\omega_1 t}+\rho_{13}e^{i\omega_1 t}). \tag{17}$$

Here A is the laser focus area, ϵ_0 is the permittivity of free space, c the velocity of light, and $n=3.6$ the refractive index of GaAs, the material surrounding the QD. In the derivation of Eq. (17) the Gouy phase is considered, which leads to a phase shift of $-\pi/2$ in the focus of a Gaussian beam.[33] Since $F_s\ll F_1$ and using the definition for the Rabi frequency Ω_1 above and the maximum transmission contrast on resonance ($\omega_1=\omega_{13}$): $\alpha_0=2e^2D_{13}^2\omega_{13}/A\epsilon_0 cn\hbar\Gamma$, we find

$$\frac{\Delta T}{T}\approx\alpha_0\frac{\Gamma}{\Omega_1}\mathrm{Im}[\rho_{13}]. \tag{18}$$

In this analysis we assume that also in the two-laser experiment, only the laser resonant with the $|1\rangle\leftrightarrow|3\rangle$ transition contributes to the differential transmission signal. The interference term from the second repump laser generally makes only a small contribution to the measured signal. To calculate ρ_{13} from Eq. (15), we consider the limit $t\rightarrow\infty$ since the usual integration times, one second or more, are significantly larger than all expected timescales in the system. In this way the signal can be calculated once any coherent Rabi oscillations have been damped away. We calculate numerically the solution for the eight optical Bloch equations in Eq. (15) with $d\rho_{ij}/dt=0$ and the condition on the occupation of the three states, $\rho_{33}=1-\rho_{11}-\rho_{22}$. The calculation leads to differential transmission spectra as a function of the systems' parameters. The spontaneous recombination rate Γ is determined experimentally from laser saturation spectroscopy and power broadening.[25] The Rabi frequencies, Ω_1 and Ω_2, are esti-

TABLE I. All parameters used to describe the data obtained from the two laser repump experiments on Dot B. The first column gives the parameter, which was modified in the experiment. In the last column, the parameter that was used to fit the theory to the data is listed.

	Ω_1	Ω_2	Γ	γ_e	γ_s	γ_2	Fit parameter
V_g	2 GHz	58 MHz	1.2 GHz	varied	35 MHz	22 MHz	γ_e
B	2 GHz	58 MHz	1.2 GHz	varied	varied	22 MHz	γ_e and γ_s
P_2	2 GHz	varied	1.2 GHz	1.2 MHz	35 MHz	22 MHz	γ_2

mated from the known laser powers.[25] This leaves the rates γ_s, γ_e, and γ_2.

V. FARADAY GEOMETRY

To gain experimental access to the transition rates connecting the three levels of the X^{1-} in a magnetic field applied parallel to the light propagating path, the Faraday geometry, we study the response of the two-laser repump experiment to the parameters that we can control *in situ*. In particular, our experimental setup allows us to control independently one or two of the interaction rates while keeping the others constant. The cotunneling rate γ_{cot} is controlled by the gate voltage as already discussed. The magnetic field changes the hyperfine interaction mediated electron spin-flip rate γ_{hf} and also, by modifying the intermixing of the electronic states, the forbidden transition rate γ_s. By studying the dependence of the repump signal on the power of the second laser and hence the Rabi frequency Ω_2, we can access the dephasing rate γ_2. The entire data set is fitted to the model in an iterative way in order to determine the individual rates. In practice, this means that the spectra of the different data sets are fitted to the theoretical model Eq. (18) repeatedly until a set of fit parameters is found that consistently describes all the data sets (see Table I). This is a laborious process but does not throw up any ambiguities: we find a unique fit to the data yielding the unknown dephasing rates to within a random error defined by the experimental signal to noise. Systematic errors arising from limitations in the model are clearly a possibility but the good fits we achieve to a large data set suggest that they are small. In the following the different experiments will be discussed. In Sec. V D the obtained values for the different rates will be presented in an overview. There also the interplay between the obtained rates will be discussed. All the Faraday geometry experiments were performed on the same QD.

A. Gate voltage dependence

In Sec. III A the gate voltage dependence of the spin-flip rate γ_e via cotunneling was shown. There we measure a change in the transmission contrast as a function of the gate voltage over the plateau. Only one laser is resonantly driving the excitonic transition [Fig. 3(b)]. In the following, we repeat the experiment in a two-laser experiment. The transmission contrast is measured with and without a second laser, repumping the optical spin polarization, for each position on the plateau. Since the repump scheme only works in case of OSP, the experiment is limited to a gate voltage range in the middle of the charging plateau. In Fig. 6(a) the measured transmission contrast is plotted against the resonance gate voltage. The solid dots represent the one-laser experiment, while the open circles were obtained by performing a two-laser experiment, with a second laser resonant with the forbidden transition. The data show clearly that the transmission contrast is always larger in a two-laser experiment. We can fit both cases for each resonance gate voltage with the model derived in Sec. IV A. To simulate the second laser being switched on and off, the Rabi frequency is set to a finite value (which we determine to $\Omega_2=58$ MHz) or to zero ($\Omega_2=0$), respectively. For a particular gate voltage, all other parameters remain fixed. We perform this fitting routine for each pair of data points by adjusting the spin-flip rate γ_e. The obtained values for γ_e are plotted in Fig. 6(b) as solid dots. As expected, the spin-flip rate increases as the gate voltage is tuned closer to the cotunneling regime. As before, we can describe this behavior with Eq. (5). The calculated spin-flip rate is the solid line in Fig. 6(b). The fitting parameters to implement Eq. (5) are, as in Sec. III A, the charging voltages $V_1=-1.085$ V and $V_2=-0.949$ V, and $\hbar\Gamma_{\mathrm{tun}}=0.05$ μeV. The calculated cotunneling rate γ_{cot} is modified by a constant term to account for the remaining hyperfine mediated spin-

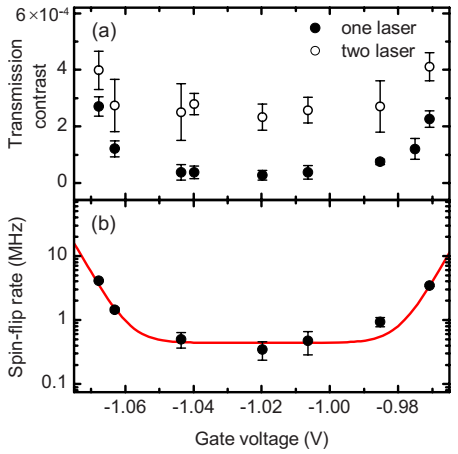

FIG. 6. (Color online) (a) Transmission contrast of a laser pumping the $|1\rangle\leftrightarrow|3\rangle$ transition with (open circles) and without (solid dots) a second laser pumping the $|2\rangle\leftrightarrow|3\rangle$ forbidden transition. All data were recorded on Dot B. A magnetic field of $B=0.5$ T was applied to obtain OSP. In (b) the spin-flip rate γ_e, obtained by fitting the quantum optical theory to the measured spectra, is plotted as a function of gate voltage. The line is a fit of Eq. (5) to the data points, with $\hbar\Gamma_{\mathrm{tun}}=0.05$ μeV. To account for the gate voltage independent hyperfine mediated spin-flip events, a constant term $\gamma_{\mathrm{hf}}=0.42$ MHz was added to γ_e [see Eq. (6)].

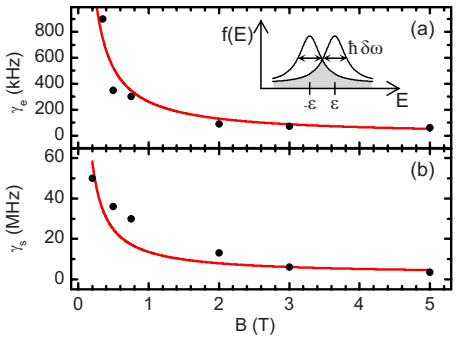

FIG. 7. (Color online) Spin-flip rate γ_e (a) and forbidden transition rate γ_s (b) as a function of the applied magnetic field. The data was obtained by fitting the quantum optical theory to the spectra measured on Dot B in one-laser and two-laser spectroscopies. The evolution of the rates with magnetic field is explained by a simple model describing electron-nuclear spin flip-flop processes. The inset in (a) illustrates the model (Ref. 34), which assumes that the strength of the hyperfine interaction is linearly related to the overlap of the electronic states $|1\rangle$ and $|2\rangle$ each broadened by $\hbar\delta\omega$ and separated by the Zeeman energy ($2\epsilon=|g_e\mu_B B|$). The ratio of the overlap region (gray) of the two Lorentzians to the whole area of the Lorentzians gives the probability of equal energy of the two spin states. With this probability, an electron spin flip can occur where the spin is transferred to a nucleus. The lines in (a) and (b) are fits of Eq. (20) to the data points with the fitting parameter $\hbar\delta\omega = 6.4$ neV, which is of the same orders of magnitude as the dephasing rate γ_2 of an electron spin in this QD. In (b) an additional offset of 2.5 MHz is added, to account for the admixture of light holes to the excitonic state.

flip rate $\gamma_{\rm hf}=0.42$ MHz [see Eq. (6)]. The tunneling energy is the same as in Sec. III A. For the other rates the following values are determined by the iterative fitting procedure: $\Gamma = 1.2$ GHz obtained from power broadening and saturation spectroscopy, $\gamma_s=35$ MHz, $\gamma_2=22$ MHz, and the Rabi frequencies are $\Omega_1=2$ GHz and $\Omega_2=58$ MHz.

The good agreement between the spin-flip rates obtained from the evaluation of the quantum optical treatment of the data and the cotunneling integral confirms the assumption that both the tunneling energy $\hbar\Gamma_{\rm tun}$ as well as the forbidden rate γ_s are to a large extent gate voltage independent.

B. Magnetic-field dependence

Similarly to the approach in the previous section, we investigate the effect of the applied magnetic field on the repump signal. The transmission contrast in a one-laser and in a two-laser experiments is measured at various magnetic fields. By fitting the quantum optical model to pairs of spectra, the values for the spin-flip rate γ_e and the forbidden transition rate γ_s were found to have a magnetic-field dependence. The results are shown in Fig. 7(a) for γ_e and Fig. 7(b) for γ_s by the solid dots. The spin-flip rate γ_e has to be varied, as well as the forbidden transition rate γ_s, to obtain good agreement between the measured and calculated spectra. We interpret the magnetic-field dependence of the forbidden transition rate as a hyperfine contribution to the rate γ_s at low magnetic fields.[8] This contribution however is strongly reduced at large magnetic fields. Finally only the magnetic-field independent contribution due to valence-band mixing remains. In the work of Dreiser *et al.*[8] this contribution was estimated to be rather small ($\approx 1\%$ of the spontaneous recombination rate). To model the hyperfine effect on the spin-flip rate γ_e and the forbidden transition rate γ_s, we use a simple intuitive model developed by Krebs.[34] We assume that the finite lifetime of the electron spin in the states $|1\rangle$ and $|2\rangle$ leads to an effective broadening of these states. Their distribution functions are given by two Lorentzians with a finite width $\hbar\delta\omega$, centered at energies $\pm\epsilon$, where $2\epsilon=E_{Z,e}$;

$$f(E) \propto \frac{2}{\pi}\frac{\hbar\delta\omega}{4(E\pm\epsilon)^2+(\hbar\delta\omega)^2}. \tag{19}$$

Because the magnetic moments of the nuclear spins are orders of magnitude smaller than the Zeeman splitting of the electrons, an electron-nuclear spin flip-flop event can only occur with the probability of finding two electrons of opposite spin at the same energy. Then both angular momentum and energy can be conserved in the flip-flop process. This probability is given by the ratio of the area of the overlap region of the two distribution functions to their total area. This is illustrated in the inset of Fig. 7(a). For the hyperfine contribution for the spin-flip rate we find,

$$\gamma_{\rm hf}(B) = \gamma_{\rm hf}^0\left[1-\frac{2}{\pi}\arctan\left(\frac{g_e\mu_B B}{\hbar\delta\omega}\right)\right]. \tag{20}$$

Here $\gamma_{\rm hf}^0$ is the hyperfine mediated spin-flip rate at zero magnetic field. We include this result in the description of the magnetic-field dependence of the spin-flip rate and the forbidden transition rate. The results are shown in Figs. 7(a) and 7(b) by the lines. In both cases, we use a constant broadening of the electron state $\hbar\delta\omega=6.4$ neV, which is of the order of the dephasing rate of the electron $\hbar\gamma_2=14.5$ neV, which we determine from the power dependence of the repump signal (Sec. V C). However the value for the dephasing rate is only an upper bound and the real spin dephasing rate might be smaller. The electron g factor is measured before, as described in Sec. III B, to be $|g_e|=0.70\pm0.01$. Considering that a constant $\delta\omega$ is possibly a rather crude description, we find a good agreement between the measured values for the rates γ_e and γ_s and the ansatz for the hyperfine interaction model. To describe the forbidden transition rate γ_s, a constant offset is added to Eq. (20): $\gamma_s=\gamma_s{\rm hf}+\gamma_s^{\rm HH-LH}$. This offset we interpret as accounting for the magnetic-field-independent contribution of the heavy-hole light-hole mixing to the forbidden transition, which is here $\gamma_s^{\rm HH-LH}=2.5$ MHz. This corresponds to an admixture of light holes into the excitonic state of $<1\%$. The rates for Γ, γ_2, and $\Omega_{1,2}$ are the same as in the previous section.

Although the hyperfine mediated spin-flip process is connected with a flip of a magnetic moment of a nucleus in the QD, we do not observe any significant nuclear-spin polarization, which would be revealed in an Overhauser shift of the excitonic resonance.

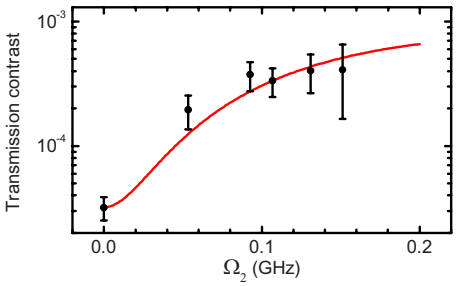

FIG. 8. (Color online) The transmission contrast of the first laser, resonant with the $|1\rangle \leftrightarrow |3\rangle$ transition, is plotted against the Rabi frequency Ω_2 of the second laser. The data were recorded on Dot B. The line is a fit of the contrast predicted by the quantum optical theory to the data points. The parameters are $\Gamma = 1.2$ GHz, $\Omega_1 = 2$ GHz, $\gamma_s = 35$ MHz, and $\gamma_e = 1.2$ MHz, and the maximum transmission contrast $\alpha_0 = 1.93 \times 10^{-3}$. From the fit, an upper bound for the dephasing rate $\gamma_2 = 22$ MHz is obtained. The experiment was performed with an external magnetic field $B = 0.5$ T applied.

C. Power dependence

To investigate the dependence of the repump signal on the power of the laser pumping the forbidden transition resonantly (P_2), the magnetic field is fixed at $B = 0.5$ T and the gate voltage at $V_G = -1.07$ V corresponding to a spin-flip rate $\gamma_e = 1.2$ MHz. Furthermore the power of the laser pumping the excitonic transition $|1\rangle \leftrightarrow |3\rangle$ is fixed corresponding to a Rabi frequency $\Omega_1 = 2$ GHz. In Fig. 8 the transmission contrast on resonance $\delta_1 = \delta_2 = 0$ [see Eq. (12)] is plotted against the Rabi frequency Ω_2.

The curve in Fig. 8 is a fit of the quantum optical model to the data. The parameters for the fit are the same as in the sections above: $\Gamma = 1.2$ GHz and the dephasing rate $\gamma_2 = 22$ MHz.

For large laser power P_2, when $\Omega_2 \approx \Omega_1$, the transmission spectra of the two-laser experiment are predicted to develop a splitting, accompanied by a reduced transmission contrast, a dip, on two-photon resonance, for instance $\delta_1 = \delta_2 = 0$. This phenomena is called electromagnetically induced transparency (EIT).[32,35] The dip arises from a destructive interference of the two transitions, first observed on Sr-atoms by Boller *et al.*[35] in 1991. In the presence of the two laser fields, the system is forced into a coherent superposition of the two ground states, called a dark state as the state does not have an optical interaction with the upper level. This coherent optical effect is of great interest in quantum information processing as it constitutes a prerequisite for purely optical coherent spin manipulation via stimulated Raman adiabatic passage (STIRAP) pump schemes.[36,37] However in our case, at laser powers strong enough to expect EIT according to the theory, the measurement is challenging because the transmission detector is over illuminated—both laser beams strike the detector—such that shot noise from the repump laser swamps the signal from the pump laser. To reach equal Rabi frequencies $\Omega_1 = \Omega_2$, here $P_2 \approx 35 P_1$ is required. In the experiment only $P_2 = 8 P_1$ is achieved with a sufficient signal-to-noise ratio.

The restriction in this aspect of the Faraday geometry experiment arises because of the vastly different spontaneous radiative decay rates, $\Gamma \gg \gamma_s$. We go on to show that this restriction can be lifted in the Voigt geometry when a magnetic field perpendicular to the growth direction is applied.[38,39]

D. Discussion

A summary of the rates, obtained from an analysis of the different experiments with the theoretical model, is given in Table I. The spontaneous decay rate of the exciton Γ is obtained by one color saturation spectroscopy and power broadening.[25] The Rabi frequency Ω_1 is directly linked to the laser power and the spontaneous decay rate of the exciton.[25] The Rabi frequency Ω_2 can be calculated from the known laser power P_2 and the forbidden transition rate γ_s. Therefore there are three remaining unknown rates: the spin-flip rate γ_e, the forbidden transition rate γ_s, and the dephasing rate γ_2. Since the three parameters we can control *in situ* (V_g, B, and P_2) correspond to these rates, we have a system of equations containing three equations and three rates. To obtain the values for these three rates, all three data sets are fit in an iterative way until a consistency between the rates and an agreement between the data and the calculated spectra is obtained.

VI. VOIGT GEOMETRY

If a magnetic field is applied in the plane of the QD (along the x direction), retaining the light propagation direction along the growth direction (Voigt geometry), the forbidden transitions become allowed. The electron and hole spins are now quantized parallel to the applied magnetic field, perpendicular to the light propagation vector, z. In the z basis, there are different electron and exciton spin eigenstates. These states are $|\tilde{1}\rangle = \frac{1}{\sqrt{2}}(|1\rangle + |2\rangle)$, $|\tilde{2}\rangle = \frac{1}{\sqrt{2}}(|1\rangle - |2\rangle)$, and $|\tilde{3}\rangle = \frac{1}{\sqrt{2}}(|3\rangle + |4\rangle)$, as well as $|\tilde{4}\rangle = \frac{1}{\sqrt{2}}(|3\rangle - |4\rangle)$. The transition between the states $|1\rangle \leftrightarrow |3\rangle$ is mediated by right-handed circularly polarized light and between the states $|2\rangle \leftrightarrow |4\rangle$ by left-handed circularly polarized light. Hence, the transitions $|\tilde{1}\rangle \leftrightarrow |\tilde{3}\rangle$ and $|\tilde{2}\rangle \leftrightarrow |\tilde{4}\rangle$ are mediated by linearly polarized light $\pi_x = \frac{1}{\sqrt{2}}(\sigma^+ - \sigma^-)$, while the transitions $|\tilde{1}\rangle \leftrightarrow |\tilde{4}\rangle$ and $|\tilde{2}\rangle \leftrightarrow |\tilde{3}\rangle$ are mediated by $\pi_y = \frac{1}{\sqrt{2}}(\sigma^+ + \sigma^-)$ and are therefore allowed. To study these transitions, the microscope was modified to perform spectroscopy in the Voigt geometry and we present a detailed series of experiments on one particular quantum dot, a different dot to that was used in the Faraday geometry.

A. High-resolution laser spectroscopy

With an in-plane magnetic field applied the unpolarized resonance line splits into four lines, as expected. In Fig. 9(a) three transmission spectra are shown, measured with three different polarizations of the laser field. The magnetic field is $B = 0.7$ T and the experiment was performed at a gate voltage in the cotunneling regime to prevent OSP. For the upmost spectrum the laser is circularly polarized and all four resonance lines are visible. With a linearly polarized laser, the inner and outer resonances can be probed selectively, as

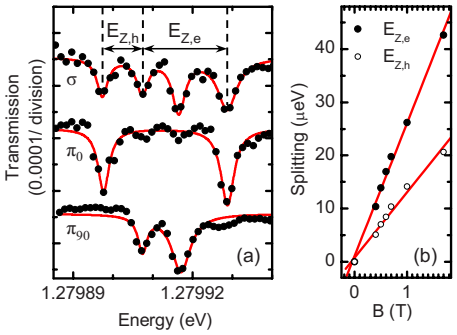

FIG. 9. (Color online) (a) One-laser transmission spectra of singly charged Dot C with an in-plane magnetic field applied ($B=0.7$ T). The three spectra were obtained for different polarizations of the laser field. For the upper curve, the laser was circularly polarized. The lower two curves were obtained for two orthogonal linear polarizations (see main text). The lines are Lorentzian fits to the data and an offset was added to the spectra for clarity. From the energy differences between the resonances, the Zeeman splitting of the electron and hole states can be calculated. In (b) these splittings are plotted as a function of the magnetic field. From a linear fit of the data points, the absolute values of the electron and hole g factors are determined to be $|g_e|=0.47$ and $|g_h|=0.24$.

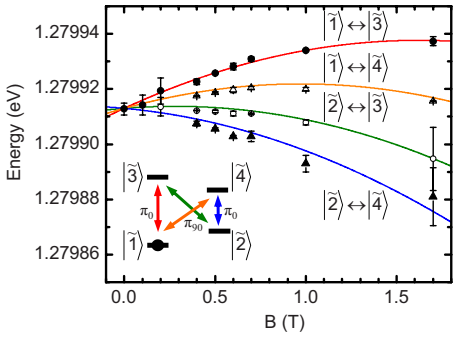

FIG. 10. (Color online) Resonance energy of the X^{1-} excitonic resonances of Dot C in Voigt geometry as a function of the magnetic field. The data points were obtained by fitting the spectra with Lorentz functions [see Fig. 9(a)]. The spectra were measured in the cotunneling regime to avoid OSP. The data points are fit by parabolas, using the g factors from Fig. 9(b) and a diamagnetic shift of -9.4 μeV/T^2. In the inset, the electronic and excitonic levels are sketched, together with the optical transitions between them.

shown in Fig. 9(a), in the middle and lower spectrum. We note that the laser light is coupled into the microscope with a normal single mode fiber so we can determine the relative angle between the two linear polarizations to be 90°, but unfortunately their angle relative to the magnetic-field direction remains unknown. However, from the polarization properties of the lines, it is reasonable to assume, first, that $\pi_0 \equiv \pi_x$ and $\pi_{90} \equiv \pi_y$, and second, the signs of the in-plane g factors of the electron and hole are negative, as in the Faraday geometry.[39] Based on this, the data allow measurements of the Zeeman splittings of the electron and hole. In Fig. 9(b) the splittings are plotted against magnetic field. From a linear fit to the measured splittings the absolute values of the g factors are acquired as $|g_e|=0.47$ and $|g_h|=0.24$. In contrast to the Faraday geometry, here the electron g factor is larger than the hole g factor. The reason for this is based on the atomic character of the electron and hole states. The electron state is built from atomic s states and the electron spin in a QD therefore follows the direction of the applied magnetic-field direction, i.e., the electron g factor is largely isotropic. Conversely, the hole state is built predominantly from heavy-hole atomic states. In the limit of zero light-hole admixture, the hole spin is expected to remain aligned along the growth direction of the QD independent of the magnetic field, i.e., the hole g factor in the Voigt geometry is zero.[40] This is of course an extreme limit but it does explain why in the Voigt geometry, the hole g factor is much smaller than in the Faraday geometry. The spectroscopic results in the Voigt geometry are summarized in the level diagram in the inset of Fig. 10 showing the allowed transitions.

The data in Fig. 10 shows the magnetic-field dependence of the resonance energies of all four resonances along with an assignment of the four transitions. The magnetic-field dependence of all four transition energies can be fitted with parabolas, yielding the diamagnetic shift -9.4 μeV/T^2. Although the magnitude of the diamagnetic shift is very similar to the diamagnetic shift measured in the Faraday geometry,[17] it is surprising that the sign of the diamagnetic shift is negative. This implies that the final state is more extended than the initial state, a fact which is not obvious in the case of a negatively charged QD in an in-plane magnetic field. It has to be stated that we have not performed a statistical study of this effect and Xu *et al.*[38] reported in a similar experiment a positive diamagnetic shift. The neutral exciton transition of the very same QD exhibits a positive diamagnetic shift (data not shown here) pointing toward a strong influence of the Coulomb interactions between the electrons and hole on the diamagnetic behavior in the Voigt geometry.

B. Optical spin pumping in Voigt geometry

As in the Faraday geometry, with an in-plane magnetic field applied, the spin of the resident electron can be optically pumped with a resonant laser field.[38] In Fig. 11(a) the transmission contrast is plotted in a grayscale plot against the gate voltage and resonance energy. The experiment was performed at $B=0.7$ T with a circularly polarized laser field (see also Fig. 9). At voltages below -0.975 V the QD is uncharged and only the neutral exciton (X^0) can be observed, energetically shifted from the X^{1-} by the electron-hole Coulomb energy. For voltages above -0.75 V the QD is charged with two electrons and resonant pumping of the s-shell transition is blocked due to the Pauli exclusion principle.[16,21] Between these voltages, one electron is trapped in the QD and the X^{1-} is accessible to resonant laser spectroscopy. At the edges of the plateau (-0.975 to -0.935 V and -0.79 to -0.75 V) the fast spin relaxation via cotunneling suppresses any significant OSP and all four transitions are visible (shown in Fig. 9). In the middle of the plateau the OSP strongly reduces the transmission contrast and no resonances are observed.

In Fig. 11(b) the result of a two-laser repump experiment is shown. For this a second laser at a constant energy 1.27997 eV and a linear π_y polarization is used. The first

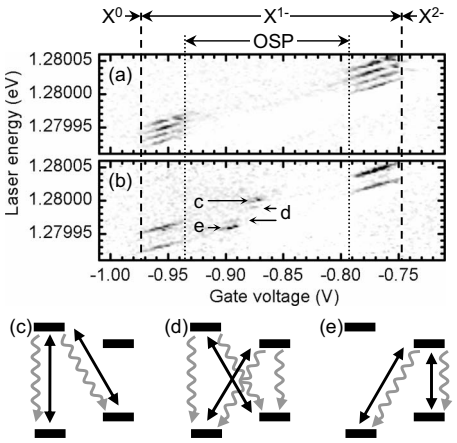

FIG. 11. OSP of the resident electron spin in a QD in Voigt geometry. The data were recorded on Dot C. (a) The transmission contrast (dark colors correspond to high transmission contrast) as a function of the gate voltage and the laser energy. The dashed lines denote the Coulomb blockade plateau, the voltage range in which the QD is charged with a single electron [compare to Fig. 3(a)]. The dotted lines mark the boundaries of the region in which the electron spin is optically pumped, leading to a much reduced transmission contrast. In between the dashed and dotted lines at the plateau edges the transmission contrast is high because of fast spin relaxation due to cotunneling [see also Fig. 3(b)]. The experiment was performed in a magnetic field of $B=0.7$ T, with a circularly polarized laser field, yielding four distinct resonances [compare to Fig. 9(a)]. In (b), a second laser at a fixed energy 1.27997 eV was additionally used. This second laser was linearly π_y polarized and the scanned laser was orthogonally polarized, along π_x. At the edges of the plateau again the signal due to cotunneling appears. In the middle of the plateau, the transmission signal of the scanned laser reappears due to optical repumping, according to the three repumping schemes (c), (d), and (e). In (c) the second, fixed laser is resonant with the $|\tilde{2}\rangle \leftrightarrow |\tilde{3}\rangle$ transition, while the scanned laser hits the $|\tilde{1}\rangle \leftrightarrow |\tilde{3}\rangle$ transition. In (d) the fixed and scanned lasers are resonant with the $|\tilde{1}\rangle \leftrightarrow |\tilde{4}\rangle$ and $|\tilde{2}\rangle \leftrightarrow |\tilde{3}\rangle$ transitions, respectively. Depending on which laser hits, which resonance at the given gate voltage, these repump signals appear as marked in (b). The recovery for the repump scheme (d) is weaker than for (c) and (e) because the polarization of the scanned laser does not match the polarization of the resonance it is pumping. In (e), similar to (c), the fixed laser is resonantly pumping the transition $|\tilde{1}\rangle \leftrightarrow |\tilde{4}\rangle$, while the scanned laser photon energy matches the $|\tilde{2}\rangle \leftrightarrow |\tilde{4}\rangle$ transition energy.

laser is scanned in energy as shown in Fig. 11(a), its linear polarization is π_x. As a result, in the cotunneling regime, only two, the high-energy and the low-energy resonances, are visible. In the middle of the plateau, the repump signal appears as a double resonance in energy at two different gate voltages. The positions are marked by arrows and labeled with (c), (d), and (e) according to the repump process, as depicted in Fig. 11. In case (c), the scanned laser is resonant with the transition $|\tilde{1}\rangle \leftrightarrow |\tilde{3}\rangle$, the energetically highest resonance in Fig. 9 (the labeling of the states follows the definition given in the inset of Fig. 10). The electron spin is shelved in state $|\tilde{2}\rangle$, but at this particular gate voltage ($V_G=-0.875$ V) the constant energy laser is resonant with the transition $|\tilde{2}\rangle \leftrightarrow |\tilde{3}\rangle$ (corresponding to the second lowest resonance energy in Fig. 9), repumping the electron into the state $|\tilde{1}\rangle$. For (e) the situation is the same except that the two other transitions are involved. The scanned laser shelves the spin via the transition $|\tilde{2}\rangle \leftrightarrow |\tilde{4}\rangle$ into state $|\tilde{1}\rangle$, while the laser with constant energy is resonant with the transition $|\tilde{1}\rangle \leftrightarrow |\tilde{4}\rangle$. The resonance condition for this case is fulfilled at a lower gate voltage $V_G=-0.895$ V because the energy of the $|\tilde{1}\rangle \leftrightarrow |\tilde{4}\rangle$ transition is higher than for the $|\tilde{2}\rangle \leftrightarrow |\tilde{3}\rangle$ transition. At both resonance voltages, weak repump signals appear at lower, (c), or higher, (e), energies. They arise from the case where the scanned laser is resonant with the $|\tilde{1}\rangle \leftrightarrow |\tilde{4}\rangle$ and $|\tilde{2}\rangle \leftrightarrow |\tilde{3}\rangle$ transitions, respectively. The scheme for this case is shown in (d). In this case the contrast is smaller than for (c) and (e) because the polarization of the scanned laser is mostly along the π_x direction. Only a small contribution, due to imperfect polarization definition, is along π_y, the polarization required to pump the transitions $|\tilde{1}\rangle \leftrightarrow |\tilde{4}\rangle$ or the transition $|\tilde{2}\rangle \leftrightarrow |\tilde{3}\rangle$.

C. Power dependence of the repump signal

In Fig. 11(b) the recovery of the transmission contrast of the laser pumping the excitonic transition $|\tilde{1}\rangle \leftrightarrow |\tilde{3}\rangle$ is achieved by a second laser, resonant with the $|\tilde{2}\rangle \leftrightarrow |\tilde{3}\rangle$ transition. This corresponds to a λ system, one of the prerequisites for EIT [Fig. 11(c)]. The difference to the Faraday geometry experiment described in Sec. V is that in Voigt geometry the two spontaneous decay rates Γ from $|\tilde{3}\rangle \rightarrow |\tilde{1}\rangle$ and γ_s from $|\tilde{3}\rangle \rightarrow |\tilde{2}\rangle$ are equal, a clear feature in the spectra shown in Fig. 9. This implies that OSP is much more efficient in the Voigt geometry than in the Faraday geometry and the laser fields couple equally well to the two optical transitions $|\tilde{1}\rangle \leftrightarrow |\tilde{3}\rangle$ and $|\tilde{2}\rangle \leftrightarrow |\tilde{3}\rangle$. Hence, for equal laser powers P_1 and P_2, the Rabi frequencies Ω_1 and Ω_2 are also equal. In this case, the quantum optical theory described above predicts a significant EIT dip provided the spin relaxation and pure spin dephasing rates are small enough. In Fig. 12 the dashed line gives the calculated transmission contrast as a function of Ω_2, for a constant $\Omega_1=2.5$ GHz and for $\Gamma=\gamma_s=4.2$ GHz. These rates are obtained from saturation spectroscopy for this QD.[25] We use the dephasing rate $\gamma_2=22$ MHz as it is obtained in Sec. V C on Dot B.

The experiment on Dot C however yields a different result, the solid dots in Fig. 12. Even for large Ω_2, which were accessible with a reasonable signal to noise, the spectra show no sign of a dip for δ_1 and $\delta_2=0$. All parameters are by this stage known apart from γ_2, the pure spin dephasing rate. The line in Fig. 12 is a fit of the theoretically calculated normalized transmission contrast for $\delta_1=\delta_2=0$ to the data points with γ_2 as fit parameter. We find $\gamma_2=6$ GHz, a value agreeing reasonably with the observed linewidth of the resonance in one-laser transmission spectroscopy. The spin-flip rate is much smaller, $\gamma_e=1.2$ MHz. Spin dephasing is therefore much faster for Dot C than for Dot B. This result tallies with our electron-spin resonance results on the same sample, in that despite almost identical optical properties, completely

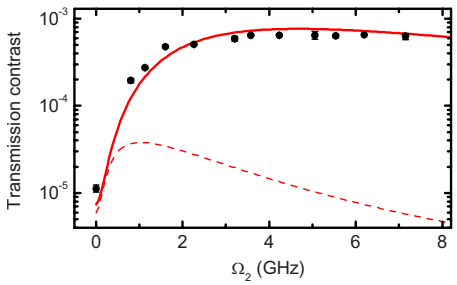

FIG. 12. (Color online) Power dependence of the repump signal in a two-laser experiment. One laser resonantly pumps the $|\tilde{1}\rangle \leftrightarrow |\tilde{3}\rangle$ transition with a Rabi frequency $\Omega_1 = 2.5$ GHz. The Rabi frequency of the second laser, resonant with the transition $|\tilde{2}\rangle \leftrightarrow |\tilde{3}\rangle$, is varied. The data were recorded on Dot C. The line represents a fit of the quantum optical theory to the data, with a dephasing rate $\gamma_2 = 6$ GHz. The other parameters are $\Gamma = \gamma_s = 4.2$ GHz, $\gamma_e = 1.2$ MHz, and $\alpha_0 = 1.8 \times 10^{-3}$. The magnetic field was $B = 0.7$ T. The Rabi frequency of $\Omega_1 = 2.5$ GHz, which leads to a power broadening and a reduced transmission contrast compared to Fig. 8, was chosen for optimum signal-to-noise ratio. The dashed line is a plot of the calculated transmission contrast expected for a dephasing rate $\gamma_2 = 22$ MHz, the upper bound determined for Dot B in Sec. V.

different spin dynamics were observed on two different QDs.[12] These effects trace back in all probability to different nuclear-spin dynamics. It would appear that to observe and exploit a pronounced EIT dip, statistics of the electron-spin dephasing rate on many QDs have to be collected and analyzed.

VII. SUMMARY AND CONCLUSION

We have performed high-resolution two-laser resonant spectroscopy on single negatively charged QDs. We demonstrate optical pumping of the spin of the resident electron in a magnetic field with one laser and the repump of the electron spin in a two-laser experiment. The experiments have been performed in both Faraday and Voigt geometries. We show that the key to unlocking the system's parameters is the repump experiment: by analyzing the response of the repump signal to bias, magnetic field, and laser power with a quantum optical model, we are able to obtain the spin relaxation and pure dephasing rates. We find that the spin T_1 time can be increased beyond a microsecond by applying a magnetic field to suppress the hyperfine interaction and working in the center of the Coulomb blockade plateau to suppress a spin swap with the back contact. However, for one dot, T_2 is less than a nanosecond; for another it is ~10 ns. This shows first, relatively fast spin dephasing, most likely via the hyperfine interaction, and second, large variations from dot to dot in the spin coherence time.

In the Voigt geometry we establish two metastable spin ground states coupled to a common excited state, a lambda system. This opens the way to observe EIT on a single quantum dot, equivalently the generation of optically dark spin state superpositions. Our work shows that the remaining stumbling block is the lack of spin coherence. We hope that this challenge can be overcome in the near future. Already, coherent population trapping has been reported in the high power limit on a negatively charged QD in Voigt geometry.[41]

ACKNOWLEDGMENTS

Financial support from the DFG (Grant No. SFB 631), German Excellence Initiative via "Nanosystems Initiative Munich" (NIM), and EPSRC-GB (U.K.) is gratefully acknowledged. We thank Jörg Kotthaus and Atac Imamoglu for the helpful discussions.

[1] A. Imamoglu, D. D. Awschalom, G. Burkard, D. P. DiVincenzo, D. Loss, M. Sherwin, and A. Small, Phys. Rev. Lett. **83**, 4204 (1999).
[2] D. Loss and D. P. DiVincenzo, Phys. Rev. A **57**, 120 (1998).
[3] A. Greilich, D. R. Yakovlev, A. Shabaev, Al. L. Efros, I. A. Yugova, R. Oulton, V. Stavarache, D. Reuter, A. Wieck, and M. Bayer, Science **313**, 341 (2006).
[4] M. Kroutvar, Y. Ducommun, D. Heiss, M. Bichler, D. Schuh, G. Abstreiter, and J. J. Finley, Nature (London) **432**, 81 (2004).
[5] M. Atatüre, J. Dreiser, A. Badolato, A. Högele, K. Karrai, and A. Imamoglu, Science **312**, 551 (2006).
[6] M. Kroner, S. Seidl, B. D. Gerardot, B. Biedermann, A. Badolato, P. M. Petroff, K. Karrai, and R. J. Warburton, Int. J. Mod. Phys. B **21**, 1307 (2007).
[7] B. Gerardot, D. Brunner, P. A. Dalgarno, P. Öhberg, S. Seidl, M. Kroner, K. Karrai, N. G. Stoltz, P. M. Petroff, and R. J. Warburton, Nature (London) **451**, 441 (2008).
[8] J. Dreiser, M. Atatüre, C. Galland, T. Müller, A. Badolato, and A. Imamoglu, Phys. Rev. B **77**, 075317 (2008).
[9] P. Maletinsky, A. Badolato, and A. Imamoglu, Phys. Rev. Lett. **99**, 056804 (2007).
[10] A. I. Tartakovskii, T. Wright, A. Russell, V. I. Falko, A. B. Vankov, J. Skiba-Szymanska, I. Drouzas, R. S. Kolodka, M. S. Skolnick, P. W. Fry, A. Tahraoui, H.-Y. Liu, and M. Hopkinson, Phys. Rev. Lett. **98**, 026806 (2007).
[11] R. I. Dzhioev and V. L. Korenev, Phys. Rev. Lett. **99**, 037401 (2007).
[12] M. Kroner, K. M. Weiss, B. Biedermann, S. Seidl, S. Manus, A. W. Holleitner, A. Badolato, P. M. Petroff, B. D. Gerardot, R. J. Warburton, and K. Karrai, Phys. Rev. Lett. **100**, 156803 (2008).
[13] H. Drexler, D. Leonard, W. Hansen, J. P. Kotthaus, and P. M. Petroff, Phys. Rev. Lett. **73**, 2252 (1994).
[14] R. J. Warburton, C. Schäflein, D. Haft, F. Bickel, A. Lorke, K. Karrai, J. M. Garcia, W. Schoenfeld, and P. M. Petroff, Nature (London) **405**, 926 (2000).
[15] J. J. Finley, A. D. Ashmore, A. Lemaitre, D. J. Mowbray, M. S. Skolnick, I. E. Itskevich, P. A. Maksym, M. Hopkinson, and T. F. Krauss, Phys. Rev. B **63**, 073307 (2001).
[16] S. Seidl, M. Kroner, P. A. Dalgarno, A. Högele, J. M. Smith, M. Ediger, B. D. Gerardot, J. M. Garcia, P. M. Petroff, K. Karrai,

and R. J. Warburton, Phys. Rev. B **72**, 195339 (2005).
[17] C. Schulhauser, D. Haft, R. J. Warburton, K. Karrai, A. O. Govorov, A. V. Kalameitsev, A. Chaplik, W. Schoenfeld, J. M. Garcia, and P. M. Petroff, Phys. Rev. B **66**, 193303 (2002).
[18] K. Karrai, R. J. Warburton, C. Schulhauser, A. Högele, B. Urbaszek, E. J. McGhee, A. O. Govorov, J. M. Garcia, B. D. Gerardot, and P. M. Petroff, Nature (London) **427**, 135 (2004).
[19] A. Högele, S. Seidl, M. Kroner, K. Karrai, C. Schulhauser, O. Sqalli, J. Scrimgeour, and R. J. Warburton, Rev. Sci. Instrum. **79**, 023709 (2008).
[20] A. Högele, M. Kroner, S. Seidl, M. Atatüre, J. Dreiser, A. Imamoglu, R. J. Warburton, A. Badolato, B. D. Gerardot, P. M. Petroff, and K. Karrai, Appl. Phys. Lett. **86**, 221905 (2005).
[21] A. Högele, S. Seidl, M. Kroner, K. Karrai, R. J. Warburton, B. D. Gerardot, and P. M. Petroff, Phys. Rev. Lett. **93**, 217401 (2004).
[22] B. Alèn, F. Bickel, R. J. Warburton, P. M. Petroff, and K. Karrai, Appl. Phys. Lett. **83**, 2235 (2003).
[23] K. Karrai and R. Warburton, Superlattices Microstruct. **311**, 33 (2003).
[24] M. Kroner, C. Lux, S. Seidl, A. W. Holleitner, A. Badolato, P. M. Petroff, R. J. Warburton, and K. Karrai, Appl. Phys. Lett. **92**, 031108 (2008).
[25] M. Kroner, S. Rémi, A. Högele, S. Seidl, A. W. Holleitner, R. J. Warburton, B. D. Gerardot, P. M. Petroff, and K. Karrai, Physica E (Amsterdam) **40**, 1994 (2007).
[26] M. Bayer, A. Kuther, A. Forchel, A. Gorbunov, V. B. Timofeev, F. Schäfer, J. P. Reithmaier, T. L. Reinecke, and S. N. Walck, Phys. Rev. Lett. **82**, 1748 (1999).
[27] M. Bayer, G. Ortner, O. Stern, A. Kuther, A. A. Gorbunov, A. Forchel, P. Hawrylak, S. Fafard, K. Hinzer, T. L. Reinecke, S. N. Walck, J. P. Reithmaier, F. Klopf, and F. Schafer, Phys. Rev. B **65**, 195315 (2002).
[28] D. Heiss, S. Schaeck, H. Huebl, M. Bichler, G. Abstreiter, J. J. Finley, D. V. Bulaev, and D. Loss, Phys. Rev. B **76**, 241306(R) (2007).
[29] J. M. Smith, P. A. Dalgarno, R. J. Warburton, A. O. Govorov, K. Karrai, B. D. Gerardot, and P. M. Petroff, Phys. Rev. Lett. **94**, 197402 (2005).
[30] L. Mandel and E. Wolf, *Optical Coherence and Quantum Optics* (Cambridge University Press, Cambridge, England, 1995).
[31] R. Loudon, *The Quantum Theory of Light* (Oxford University Press, Oxford, 2000).
[32] M. Fleischhauer, A. Imamoglu, and J. P. Marangos, Rev. Mod. Phys. **77**, 633 (2005).
[33] L. G. Gouy, Acad. Sci., Paris, C. R. **110**, 1251 (1890).
[34] O. Krebs (private communication).
[35] K. J. Boller, A. Imamoglu, and S. E. Harris, Phys. Rev. Lett. **66**, 2593 (1991).
[36] J. R. Kuklinski, U. Gaubatz, F. T. Hioe, and K. Bergmann, Phys. Rev. A **40**, 6741 (1989).
[37] U. Gaubatz, P. Rudecki, S. Schiemann, and K. Bergmann, J. Chem. Phys. **92**, 5363 (1990).
[38] X. Xu, Y. Wu, B. Sun, Q. Huang, J. Cheng, D. G. Steel, A. S. Bracker, D. Gammon, C. Emary, and L. J. Sham, Phys. Rev. Lett. **99**, 097401 (2007).
[39] M. Bayer, O. Stern, A. Kuther, and A. Forchel, Phys. Rev. B **61**, 7273 (2000).
[40] W. Sheng and P. Hawrylak, Phys. Rev. B **73**, 125331 (2006).
[41] X. Xu, B. Sun, P. R. Berman, D. G. Steel, A. S. Bracker, D. Gammon, and L. J. Sham, arXiv:0805.2074, Nat. Phys. (to be published).